Structural characterization of heat-treated activated carbon fibers

A. M. Rao[a)]
Department of Physics, Massachusetts Institute of Technology, Cambridge, Massachusetts 02139

A. W. P. Fung
Department of Electrical Engineering and Computer Science, Massachusetts Institute of Technology, Cambridge, Massachusetts 02139

M. S. Dresselhaus
Department of Electrical Engineering and Computer Science and Department of Physics, Massachusetts Institute of Technology, Cambridge, Massachusetts 02139

M. Endo
Faculty of Engineering, Department of Electrical Engineering, Shinshu University, Nagano 380, Japan

(Received 10 January 1992; accepted 13 March 1992)

Raman scattering, x-ray diffraction, and BET measurements are used to study the effect of heat treatment on the microstructure of activated carbon fibers (ACFs) and to correlate the structural changes with the metal-insulator transition observed in the electronic transport properties of heat-treated ACFs. A sequence of events is identified, starting with desorption, followed by micropore collapse plus the stacking of basic structural units in the *c*-direction, and ending up with in-plane crystallization. The graphitization process closely resembles that depicted by Oberlin's model, except that the final material at high-temperature heat treatment remains turbostratic. Because the metal-insulator transition was observed to occur at heat-treatment temperature $T_{HT} \simeq 1200$ °C, which is well below the T_{HT} value (2000 °C) for in-plane crystallization, we conclude that this electronic transition is not due to in-plane ordering but rather to the collapse of the micropore structure in the ACFs. Raman scattering also provides strong evidence for the presence of local two-dimensional graphene structures, which is the basis for the transport phenomena observed in heat-treated ACFs.

I. INTRODUCTION

Activated carbon fibers (ACFs) are highly disordered materials with a high potential for industrial applications because of their large surface areas. ACFs also provide a suitable system for testing scientific theories that have been proposed for highly disordered materials.[1] Due to their large specific surface area (SSA) of nearly 3000 m^2/g, the ACFs have a large density of defects that play an important role in their transport and optical properties, and give rise to photoconductivity and localization effects.[2,3] Their huge SSA has made ACFs a good adsorption agent for solvents and gases, and a useful material for making double layer capacitors.[4]

Preliminary measurements of the temperature dependence of the electrical conductivity and magnetoresistance,[1,3] photoconductivity,[2] and Raman spectra[5] of ACFs have previously been carried out to obtain insight into the transport mechanism and the role of defects in the transport properties of ACFs. For highly disordered and inhomogeneous materials such as ACFs, it is necessary to characterize their physical properties by several experimental techniques so that the complementary information thus obtained can be correlated to yield detailed information on the microstructure of ACFs.

Recently Fung *et al.*[6] and Kuriyama *et al.*[7,8] have carried out, respectively, preliminary studies of the electrical transport and photoconductivity properties of ACFs subjected to various heat-treatment temperatures (T_{HT}). Both studies lead to consistent conclusions regarding the electronic structure of ACFs as a function of T_{HT}. Both studies show that the ACFs exhibit a greater degree of graphitization with increasing T_{HT} and the ACFs undergo an electronic phase transition for $T_{HT} \sim 1200$ °C. As a consequence of heat treatment, the electrical transport measurements[6] show six drastic changes induced by the electronic phase transition: (1) a decrease in the absolute value of the resistivity by several orders of magnitude, depending on the measurement temperature ($T \leqslant 300$ K), (2) a major change in the functional form of the resistivity as a function of measurement temperature, (3) an increase in the zero-temperature electrical conductivity value from zero to a finite value, (4) a sign change in the dependence of the conductivity on disorder, (5) a transition from positive to negative magnetoresistance, and (6) an appearance of anisotropy in the magnetoresistance data. Likewise, from the photoconductivity experiments,[7,8] a rapid decrease in

[a)]Present address: Department of Physics and Astronomy, University of Kentucky, Lexington, Kentucky 40506.

photoconductivity was observed when T_{HT} was increased above about 1000 °C, suggesting the development of a pregraphitic structure as T_{HT} is increased into this range. Fast carrier recombination occurs for delocalized carriers that populate the pregraphitic regions, and consequently no photoconductivity is observed for single crystal graphite or in graphites with delocalized carriers.

It is well established that the effect of heat treatment on as-prepared vapor-grown carbon fibers is to graphitize the fibers, leading to the growth of a highly crystalline graphite structure.[9] Raman scattering has been used as a powerful tool for characterizing the graphitization process in benzene-derived fibers (BDFs)[9] in the near-surface region (to a depth of ~600 Å).

A more complete picture of the graphitization process in carbonaceous materials was provided by Oberlin[10] using results obtained from a variety of characterization tools including x-ray diffraction, optical microscopy, Transmission Electron Microscopy (TEM), and infrared spectroscopy. It was found that in the graphitization process, basic structural units (BSUs) are formed initially. For $T_{HT} < 800$ °C, the release of heteroatoms allows adjacent BSUs to get close enough to each other to form distorted columns. These columns are, however, independent and are only approximately parallel to one another because of the presence of some single misoriented BSUs trapped between columns. These trapped BSUs begin to align when T_{HT} gets above 1500 °C, and adjacent columns can then get hooked to one another, edge to edge, and distorted wrinkled layers thus form. The microcrystallite size in the *c*-axis (L_c) also grows very fast in the range 1500 °C < T_{HT} < 1900 °C. Above T_{HT} = 1700 °C, the in-plane zigzag-like boundary defects are annealed away. In the range 1900 °C < T_{HT} < 2100 °C, dewrinkling takes place rapidly and finally at $T_{HT} > 2100$ °C, the layers become stiff and crystalline, with nearly all of the in-plane defects removed. It is worth noting that nongraphitizing carbons follow the same graphitization path, although they cannot achieve as high a final degree of graphitization as graphitizing carbons, because their elemental domains in the bulk mesophase (pore walls) are much smaller before graphitization.[10]

In this paper, both Raman scattering studies and x-ray diffraction studies are used to obtain the in-plane crystallite size (L_a) and the *c*-axis d_{002} interlayer distance for the ACFs subjected to various T_{HT}. These structural parameters are both sensitive to the graphitization process. BET measurements are used to characterize the SSA of the ACFs as a function of T_{HT}. The goals of this study are to determine whether ACFs follow the same graphitization process as that described by Oberlin[10] and to relate the electronic phase transition observed in the temperature-dependent resistivity, magnetoresistance, and photoconductivity for T_{HT} between 1000 °C and 1200 °C to some kind of a structural transformation of the ACFs that takes place as a result of heat treatment. Because the SSA can be used as a parameter to characterize the porosity and disorder, which change drastically upon heat treatment, BET measurements are presented first to provide a common starting point for our discussion of other characterization techniques.

II. EXPERIMENTAL DETAILS

The precursor material of the ACFs used in this study is isotropic pitch that is spun to form a fiber. The average diameter for the as-spun fibers is ~10 μm and the fibers were activated by heating them at 800–1200 °C in the presence of CO_2 or water vapor. Pitch-based ACFs with SSAs of 1000 m^2/g, 2000 m^2/g, and 3000 m^2/g were obtained by controlling the activation times and temperatures. The SSA was determined by BET analysis of the adsorption isotherm of N_2 at 78 K and of CO_2 at 195 K.[11]

An argon-ion laser operating at 4880 Å was used in the Raman backscattering geometry to provide ~50 mW of incident radiation at the sample. The fiber bundle was held on a Pyrex glass slide by wrapping the ends of the fibers with parafilm strips. The central portion of the bundle was exposed to 50 mW laser radiation. The scattered radiation was collected by a 50 mm camera lens and focused onto the entrance slit of a SPEX-1403 spectrometer. Similar sample preparation techniques were used for x-ray diffraction experiments and the central region of the fiber bundle was exposed to Cu-K_α radiation in a Diano diffractometer.

III. BET CHARACTERIZATION

BET measurements are shown as points in Fig. 1 for ACFs heat-treated to various T_{HT}. To justify why these points were joined by the solid lines, the curve of SSA against T_{HT} for activated carbon fiber cloth[12] is also shown. As T_{HT} is increased, the SSAs for all the fibers show a precipitous drop in SSA from that for the as-prepared fibers to very small values for high T_{HT}.

We observe in the same figure that the higher the initial SSA, the higher the T_{HT} needed to produce a collapse in the pore volume. One possible explanation is that the as-prepared ACFs with higher initial SSA tend to have, before heat treatment, a larger proportion of thin, single graphene layer platelets, and the misorientation angles between neighboring graphite platelets are more likely to be larger because of the enhanced degrees of freedom associated with a larger number of pores. During the heat-treatment process, trapped adsorbed species have to be desorbed from the system first, before the platelets can get realigned. This is corroborated by an ESR study[13] which shows that for $T_{HT} < 450$ °C, a narrow peak, due to dangling bonds, appears in the ESR spectrum

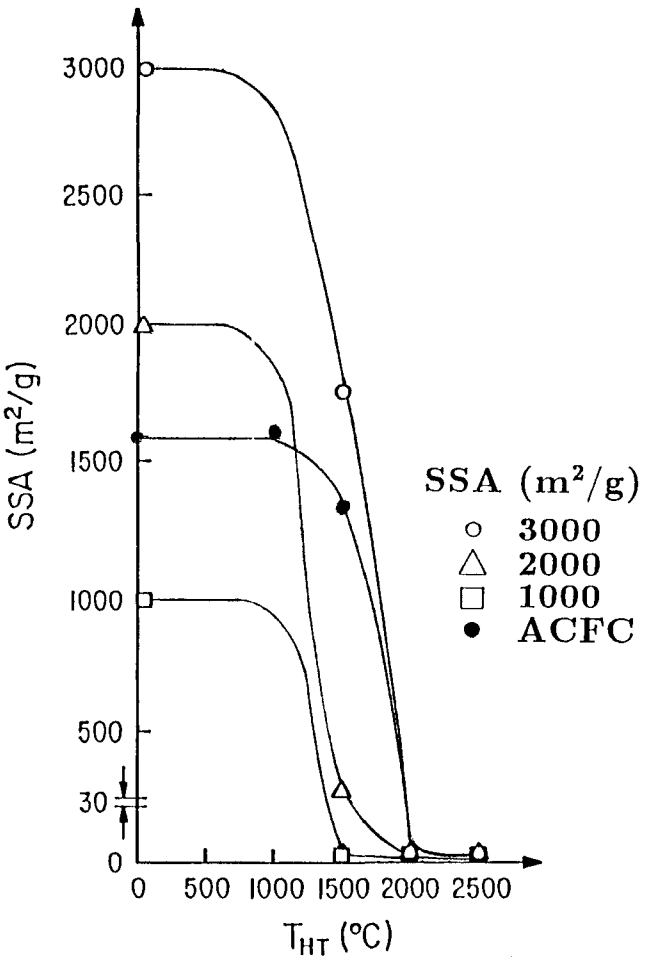

FIG. 1. Plot of SSA for the ACFs as a function of T_{HT}. The solid curves indicate the drop in SSA value for the ACFs when subjected to heat-treatment temperatures up to ~2500 °C. The curves are drawn to have the same shape as the solid curve for activated carbon fiber cloth (ACFC).[12]

for the pitch-based ACFs with SSA = 3000 m^2/g. The appearance of the dangling bonds on the surface can be attributed to the desorption of adsorbed species. With thick platelets, which are more or less aligned (at least with respect to the *c*-axis), the process of desorption should involve diffusion mainly and should resemble that of deintercalation,[14] a relatively easy process compared with the capillary action of driving the gas out through small ducts formed between the micropores bound by platelets one layer thick.

The BET data in Fig. 1 suggest that the pore size decreases in ACFs as a result of increasing T_{HT} to 2000 °C. Beyond 2000 °C, there is negligible change in the SSA of ACFs largely because of the low SSA values for $T_{HT} \geqslant 2000$ °C.

IV. X-RAY CHARACTERIZATION

In order to study the structural ordering along the *c*-direction in ACFs, room-temperature d_{002} x-ray diffraction profiles were measured for the various types of heat-treated ACFs. Figure 2 shows the d_{002} diffraction profiles for ACFs with SSA =1000 m^2/g heat-treated to various T_{HT}. The width of the (002) diffraction peak is very broad for the ACFs with low T_{HT} but it becomes sharper with increasing T_{HT}. Also, the value of the peak position for the (002) peak upshifts in 2θ values for increasing T_{HT}, indicating a decrease in the interlayer distance between the graphene layers. We believe that the broad (002) diffraction peak is composed of a range of contributions, each corresponding to a different d_{002} value in the structure of ACFs. Indeed, in the diffraction spectra for 3000 m^2/g ACFs heat-treated above 2000 °C, the diffraction profile clearly indicates the presence of several distinct peaks, but we could not resolve each of them experimentally.

The observation of a range of discrete d_{002} spacings is consistent with previous diffraction experiments in disordered graphite.[15,16] The sharpening of the (002) diffraction peak width with increasing T_{HT} suggests that the BSUs in the ACFs become better aligned with respect

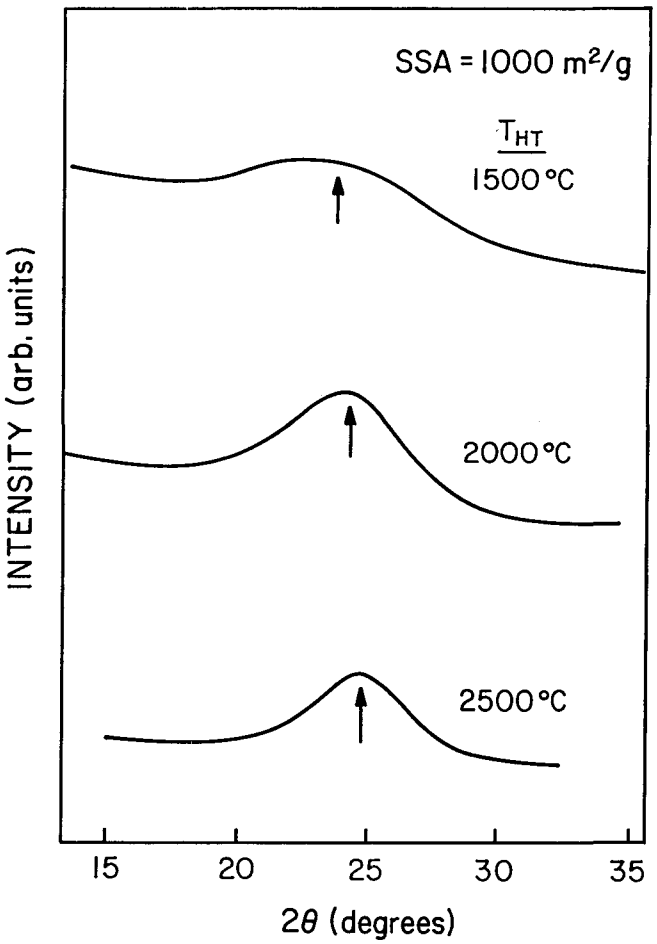

FIG. 2. The x-ray diffraction profiles for ACFs with SSA = 1000 m^2/g heat-treated to various T_{HT} values. The peak positions are indicated by arrows.

to each other and larger in size in the direction of the *c*-axis as T_{HT} increases. The results further indicate that the distribution in *d*-spacings in the ACFs narrows when the ACFs are heat-treated to 2500 °C. Recently, Aladekomo and Bragg[16] have investigated in detail the factors that cause distortion of the x-ray diffraction line profiles in carbons by analyzing the diffraction profiles of mechanically ground graphite. Their study shows that the mechanical grinding of graphite continuously increases the interlayer spacing in the range 3.354 Å $\leqslant d_{002} \leqslant$ 3.375 Å and widens the distribution of *d*-spacings. Further grinding caused discontinuous transformations of the material, forming metastable phases characterized by interlayer spacings of 3.40 Å, 3.49 Å, and 3.55 Å.

To characterize the ACFs, we used the simple centroid method to determine the average $\langle 2\theta \rangle$ of the x-ray data, as shown in Fig. 2. The average d_{002} interlayer spacing was then obtained from Bragg's formula. Representative d_{002} interlayer distances are plotted as points in Fig. 3 for the ACF samples used in this study. Irrespective of the SSA, the interlayer spacing decreases in ACFs with increasing T_{HT}. Solid, dashed, and dotted lines are passed through the points to show the trends in the decrease of the d_{002} spacing for the 3000, 2000, and 1000 m^2/g SSA fibers, respectively. Even for heat-treatment temperatures of 2500 °C, the d_{002} interlayer spacing is ~3.5 Å, indicating that the structure of the heat-treated ACFs remains in the turbostratic regime. The rate of change of the d_{002} spacing with T_{HT} is the fastest for the ACFs with SSA of 3000 m^2/g, most probably because in this range of T_{HT}, the micropores in the 3000 m^2/g fibers may just be beginning to collapse

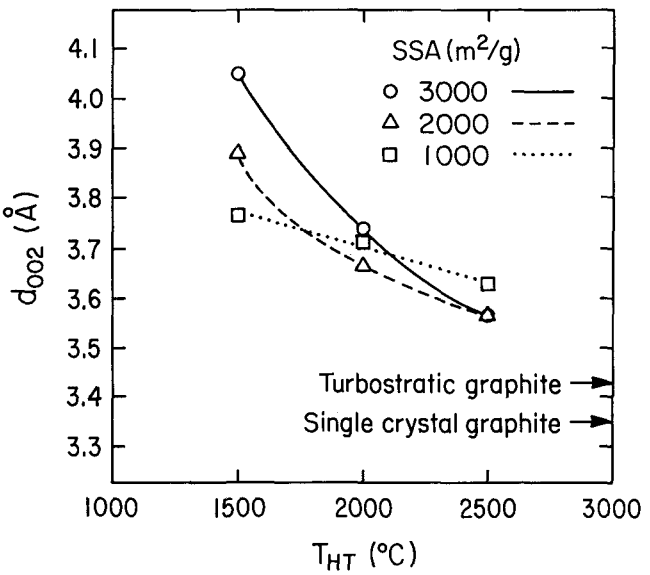

FIG. 3. d_{002} interlayer distances obtained using the centroid method and Bragg's formula for ACFs heat-treated to various T_{HT}. Also indicated on the figure (by arrows) are the d_{002} values for single crystal and turbostratic graphite.

whereas the porosity of the ACFs with lower initial SSA has already been reduced to very low values.

The information obtained from the x-ray experiment (Fig. 3) and the BET experiment (Fig. 1), when correlated, suggests that heat treatment reduces the misorientation angle between the BSUs, thereby closing up the micropores that contribute most importantly to the SSA of ACFs. With the reduction in misorientation angle, the graphene layers can grow and the interplanar distances can decrease. However, because the initial size of the BSUs is very small (about 10 Å thick and 20 Å wide in-plane), ACFs cannot be completely graphitized. Furthermore, the activation process naturally involves chemisorption of oxygen, which dehydrogenates the material, thereby depleting the ACF system of the CH groups that enhance graphitizability. With particular relevance to the present study is the observation that the collapse of the pore structure occurs at much lower T_{HT} than the formation of large in-plane platelets, as revealed by the Raman scattering experiments discussed below.

V. RAMAN CHARACTERIZATION

Room-temperature Raman spectra for ACFs with SSA values of 2000 m^2/g are shown in Fig. 4 for the as-prepared fibers and for fibers with T_{HT} values of 1500 °C, 2000 °C, and 2500 °C. Similar spectra were obtained for the 1000 m^2/g and the 3000 m^2/g fibers and are not shown in Fig. 4. The spectra in Fig. 4 show two distinct peaks, namely, the disorder-induced (*D*) peak at ~1360 cm^{-1} and the E_{2g_2} Raman-allowed graphitic (*G*) peak at ~1580 cm^{-1}. The 1580 cm^{-1} *G* line is associated with the zone-centered phonon whereas the 1360 cm^{-1} *D* line arises from the presence of a high density of phonon states near ~1360 cm^{-1} for graphite. In the presence of disorder, the selection rules for Raman-active modes are relaxed and thus non-zone-centered peaks such as the 1360 cm^{-1} peak can be observed.[17]

We note two main features of the lines in Fig. 4: (1) The intensity of the disorder-induced *D* peak at ~1360 cm^{-1} decreases with increasing T_{HT} relative to that of the 1580 cm^{-1} *G* peak. (2) The half-width-at-half-maximum (HWHM) intensity linewidth of the 1580 cm^{-1} *G* peak decreases with an increase in T_{HT}. These two features are also observed in the Raman spectra for the 1000 m^2/g and 3000 m^2/g ACFs although the detailed T_{HT} dependence of the line intensities and linewidths is sensitive to the SSA of the ACFs.

From a Lorentzian fit to the data in Fig. 4, important information about the microstructure of the fibers can be obtained. Similar experiments and analyses were used by Chieu *et al.*[9] in studying the microstructure of the benzene-derived vapor-grown fibers (BDFs), and a measure of the in-plane crystallite size (L_a) was obtained

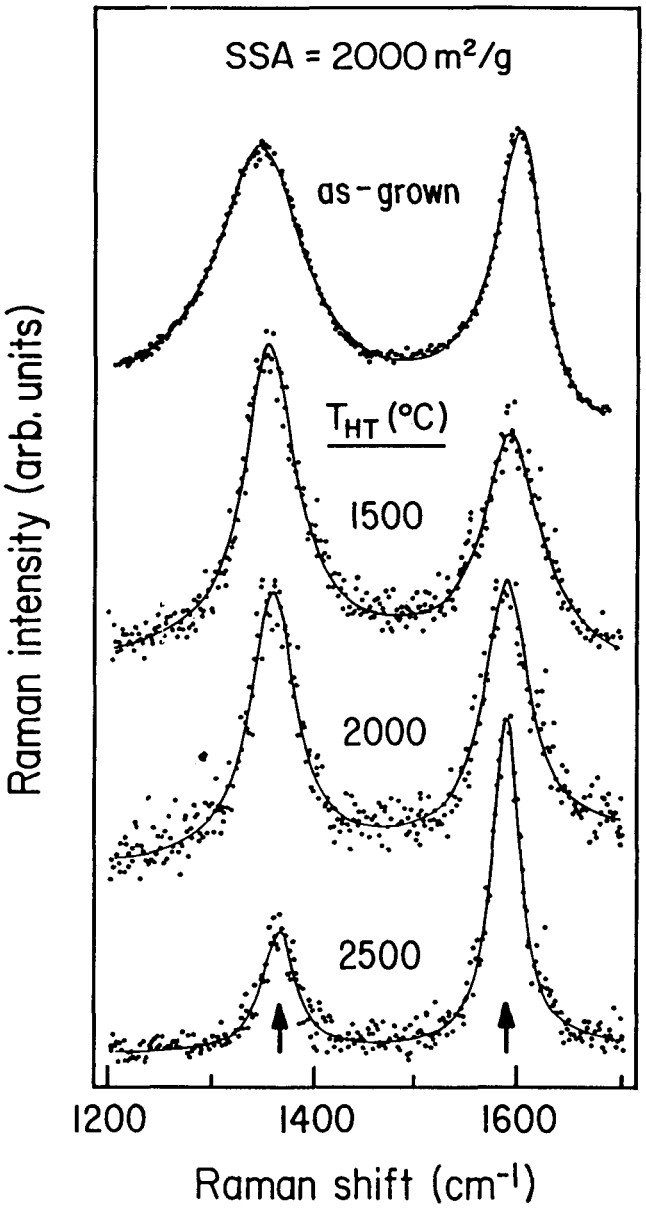

FIG. 4. Room-temperature Raman spectra for the 2000 m^2/g ACFs, including the as-prepared fibers and for T_{HT} values of 1500 °C, 2000 °C, and 2500 °C. The solid curves are the Lorentzian fits to the data. The D and G peak positions are indicated by arrows.

for the heat-treated BDFs as a function of T_{HT}. When T_{HT} was increased to ~3000 °C, the intensity of the 1360 cm^{-1} line in BDFs was reduced to very small values, as individual crystallites become well aligned with respect to the neighboring crystallites and the microstructure of the BDFs becomes close to that of HOPG.[9]

The first study correlating the Raman data with x-ray data for disordered graphite was performed by Tuinstra and Koenig[18] and they used the relative ratio (R) of the integrated intensities for the D and G (1360 cm^{-1} and 1580 cm^{-1}) lines to provide a measure of L_a. More recently, from a comprehensive study of the ratio R obtained from Raman scattering experiments in different carbon materials, Knight and White[19] obtained the empirical relation between L_a and R given as

$$L_a(\text{Å}) = \frac{44}{R}. \quad (1)$$

Figures 5(a) and 5(b) are plots of R and L_a, respectively, for our ACFs as a function of T_{HT}. In Fig. 5(b) the dotted, dashed, and solid curves act as a guide to the eye and show the changes in L_a as a function of T_{HT} for the 1000 m^2/g, 2000 m^2/g, and the 3000 m^2/g ACFs, respectively. In Fig. 5, the changes in R and L_a for ACFs are also compared with those obtained by Chieu *et al.*[9,18] for BDFs.

The results of Figs. 5(a) and 5(b) indicate that, irrespective of the SSA, the ACFs show a considerable degree of graphitization and exhibit similar behavior for the in-plane structure to that found for the BDFs for increasing T_{HT}. It is interesting to note in Fig. 5(b) that L_a is only weakly sensitive to SSA for $T_{HT} <$ 2000 °C, consistent with our Raman study of as-prepared ACFs with different SSAs.[3] On the other hand, for $T_{HT} >$ 2000 °C, the 3000 m^2/g fibers show a significant increase in L_a, while the increase in L_a is less pronounced for the 2000 m^2/g and 1000 m^2/g fibers.

This behavior of L_a for the 3000 m^2/g fibers can be related to the resistivity results,[6] which suggested that ACFs with a low SSA tend to be more graphitizable than those with a high SSA. The ACFs studied previously[6] had SSA only up to 2000 m^2/g and according to Fig. 5, those fibers should have essentially the same values for L_a.

As a further check on the graphitization of ACFs with increasing T_{HT}, we plot in Figs. 6(a) and 6(b) the HWHM intensity linewidth and the peak position of the Raman allowed 1580 cm^{-1} mode for different SSA values, as given in the legend. As in Figs. 5(a) and 5(b), comparisons of the HWHM linewidths and the Raman-allowed frequency positions of ACFs with those of BDFs[9] show similar trends for increasing T_{HT}, indicating that such highly disordered ACFs are surprisingly graphitizable, but still not nearly as graphitizable as the BDFs,[9] which extrapolate to the HWHM and Raman frequency values of highly oriented pyrolytic graphite (HOPG) with increasing T_{HT}, as shown in Fig. 6. Indeed, the linewidths for ACFs remain significantly larger at T_{HT} = 2500 °C than for BDF, consistent with the notion that disordered systems tend to have a larger variation of the atomic environments for various carbon atoms. Despite the large error bars, these results show that the ACF material becomes reasonably ordered at T_{HT} = 2500 °C, as evidenced by the large L_a values plotted in Fig. 5(b), and therefore Raman scattering may become a sensitive characterization tool for these materials with high T_{HT}.[20]

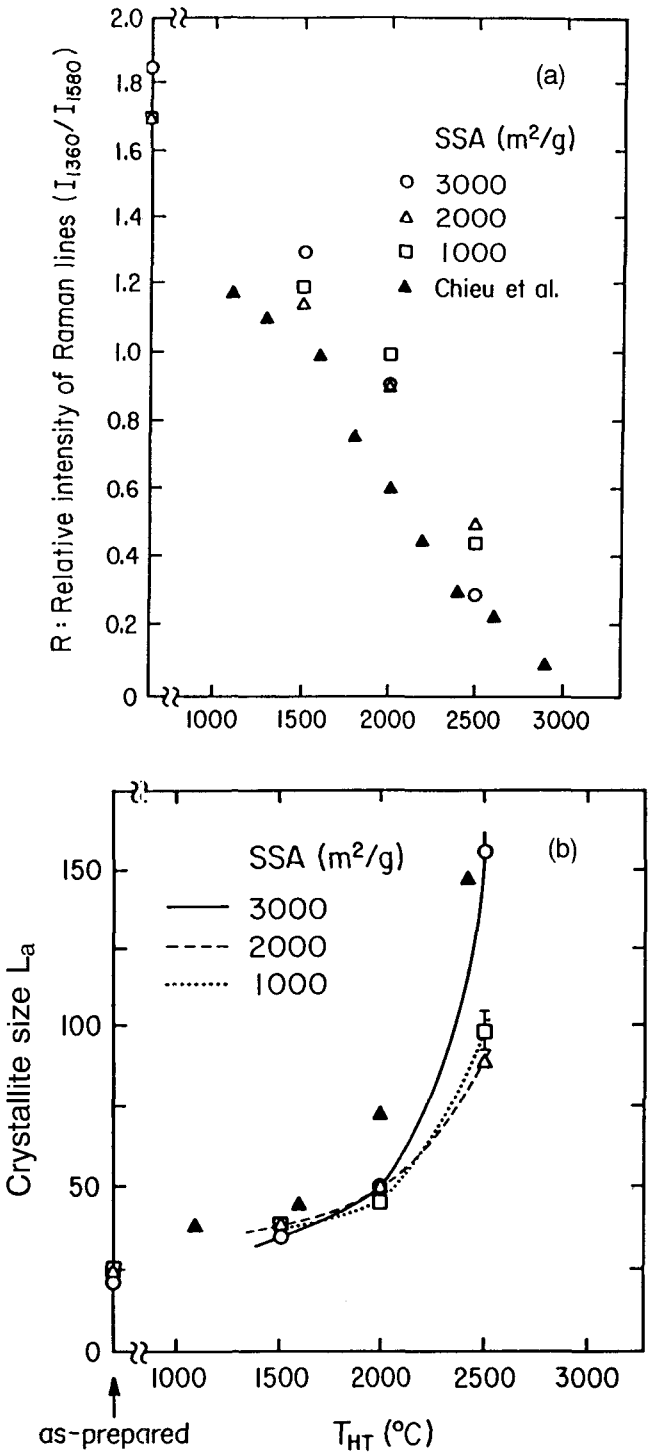

FIG. 5. Plots of the (a) relative integrated intensity of Raman lines R and (b) in-plane crystallite size L_a for ACFs as a function of T_{HT}. In (b) the solid, dashed, and dotted curves act as a guide to the eye and show the changes in L_a for increasing T_{HT} for the 3000 m^2/g, 2000 m^2/g, and the 1000 m^2/g fibers, respectively. For comparison, the corresponding data for benzene-derived vapor-grown fibers are also shown.

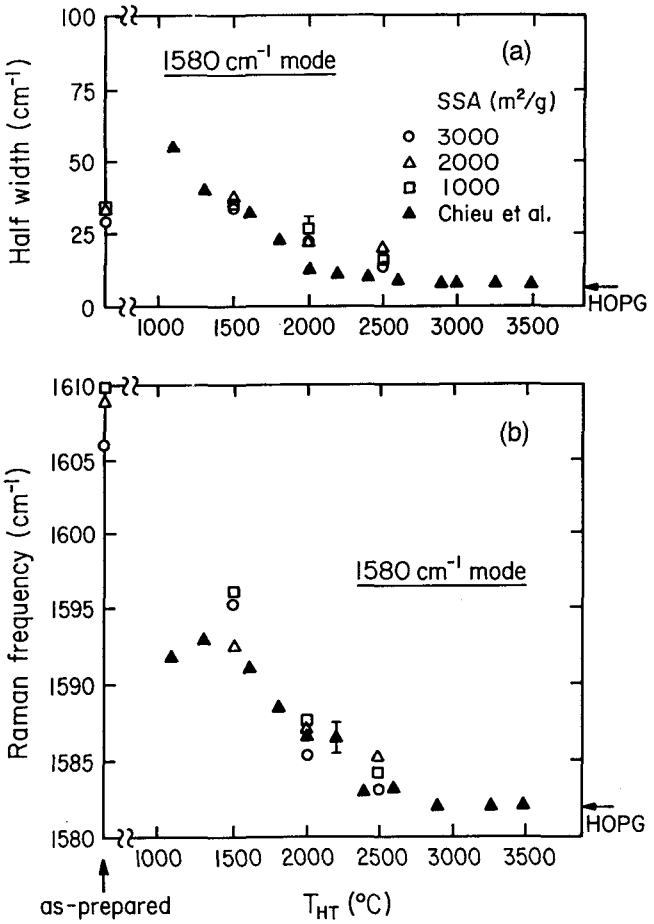

FIG. 6. Plots of the (a) HWHM linewidth and the (b) Raman frequency for the 1580 cm^{-1} mode for ACFs as a function of T_{HT}. For comparison, similar results are shown for BDFs, for which the data extrapolate to the HWHM linewidth and Raman frequency values for HOPG.[9] The legend gives the identification of the fibers according to T_{HT} and SSA.

The relative trends of the HWHM linewidths and Raman frequencies with respect to SSA may be indicative of the relationship between disorder and SSA upon heat treatment. It appears in Fig. 6 that the ACFs that have a higher SSA and more disorder before heat treatment graphitize more completely. As shown in Fig. 6 even for the most highly graphitized ACFs, they still remain turbostratic with regard to interplanar correlations after heat treatment, in agreement with Fig. 3.

VI. DISCUSSION AND CONCLUSIONS

To draw connections with the transport results,[6] we note that Raman scattering spectra do provide evidence for the growth of local two-dimensional graphene platelets in ACFs with increasing T_{HT}. The six drastic changes revealed in the transport results (see Sec. I) can mostly be explained by considering the heat-treated ACF system as a poor metal. The formation of microcrystalline graphite justifies such a treatment.

More importantly, when the results from all three characterization experiments are correlated, the sequence

of events that happens in the course of graphitization induced by heat treatment can be identified. To complete our understanding, we also refer to results from an ESR study of ACFs[13] which shows that under heat treatment at $T_{HT} < 450$ °C, desorption of adsorbed gases first takes place. Then, our BET and x-ray results provide direct and indirect evidence for the collapse of micropores upon heat treatment at some T_{HT} value much lower than 2000 °C (see Fig. 1), depending on the SSA and T_{HT} values of the ACFs. At these T_{HT} values, the basic structural units begin to stack along the *c*-axis, forming independent distorted columns. The interplanar distance decreases as the stacking continues and the columns begin to associate edge to edge with increasing T_{HT}. When T_{HT} exceeds 2000 °C, in-plane order begins to develop as the waviness is reduced and L_a increases. Because the as-prepared ACF material initially contains a lot more micropores and adsorbed oxygen than graphitizing carbons, ACFs cannot be completely graphitized and the turbostratic structure remains, consistent with the interlayer distance measured by x-ray diffraction (>3.44 Å). We conclude that the graphitization process in ACFs follows the same sequence of events as described by Oberlin,[10] except for the final formation of flat polycrystalline graphite with three-dimensional ordering which does not occur for ACFs. The microstructural change in ACFs under heat treatment can be illustrated by the schematic representation of nongraphitizing [Fig. 7(a)] versus graphitizing [Fig. 7(b)] structures of activated carbon (figures extracted from Ref. 21). ACFs should have a microstructure similar to that shown in Fig. 7(a) before heat treatment. After heat treatment at high T_{HT}, the pores disappear, leaving a layered microstructure, as shown in Fig. 7(b). The layers are, however, still turbostratic, i.e., uncorrelated with one another along the *c*-axis.

In Figs. 5 and 6, we note that the effect of heat treatment on the development of full crystallinity in the benzene-derived fibers diminishes only after T_{HT} reaches 3000 °C and beyond.[9] It would therefore be of interest to heat-treat our ACFs to temperatures of 3500 °C to find out about the ultimate degree of crystallinity achievable in ACFs by heat treatment.

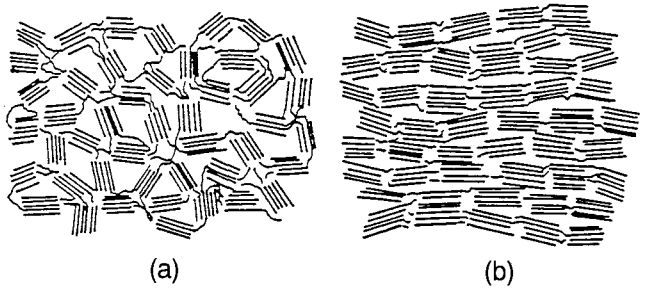

FIG. 7. A schematic representation of the microstructures of (a) nongraphitizing and (b) graphitizing activated carbons. Figures (a) and (b) are used to illustrate the microstructures of ACFs before and after heat treatment, respectively (figures extracted from Ref. 21).

All the transport studies of the effect of heat treatment on ACFs have provided evidence for a metal-insulator transition at a transition temperature of about 1000 °C to 1200 °C. It is therefore concluded that the metal-insulator transition is related to the collapsing of the micropores within these fibers and is not related to the long range in-plane development of crystalline order which happens above $T_{HT} \sim 2000$ °C.

ACKNOWLEDGMENTS

We are grateful to Dr. G. Dresselhaus for his continuing interest in this work. We are thankful to the Lawrence Livermore National Laboratory for support of this research under DOE subcontract #B130530.

REFERENCES

1. S. L. di Vittorio, M. S. Dresselhaus, M. Endo, J. P. Issi, L. Piraux, and V. Bayot, J. Mater. Res. **6**, 778 (1991).
2. K. Kuriyama and M. S. Dresselhaus, J. Mater. Res. **6**, 1040 (1991).
3. A. W. P. Fung, A. M. Rao, K. Kuriyama, M. S. Dresselhaus, and G. Dresselhaus, in *Defects in Materials*, edited by P. D. Bristowe, J. E. Epperson, J. E. Griffith, and Z. Liliental-Weber (Mater. Res. Soc. Symp. Proc. **209**, Pittsburgh, PA, 1991), p. 335.
4. M. Endo, Y. Okada, and H. Nakamura, Synth. Met. **34**, 739 (1989).
5. A. M. Rao, A. W. P. Fung, M. S. Dresselhaus, G. Dresselhaus, and M. Endo, in *Extended Abstracts of the 20th Biennial Conference on Carbon,* page 242, 1991, Santa Barbara, CA.
6. A. W. P. Fung, A. M. Rao, K. Kuriyama, M. S. Dresselhaus, G. Dresselhaus, and M. Endo, in *Extended Abstracts of the 20th Biennial Conference on Carbon,* page 296, 1991, Santa Barbara, CA.
7. K. Kuriyama, M. S. Dresselhaus, and A. W. P. Fung, in *Extended Abstracts of the 20th Biennial Conference on Carbon,* page 300, 1991, Santa Barbara, CA.
8. K. Kuriyama and M. S. Dresselhaus, J. Mater. Res. **7**, 940 (1992).
9. T. C. Chieu, M. S. Dresselhaus, and M. Endo, Phys. Rev. B **26**, 5867 (1982).
10. A. Oberlin, Carbon **22**, 521 (1984).
11. E. Tanaka, Fuel and Combustion **54**, 241 (1987).
12. I. Tanahashi, A. Yoshida, and A. Nishino, J. Appl. Electrochem. **21**, 28 (1991).
13. S. L. di Vittorio, M. S. Dresselhaus, T. Enoki, M. Endo, and T. Nakajima (unpublished).
14. M. S. Dresselhaus and G. Dresselhaus, Adv. Phys. **30**, 139 (1981).
15. J. Lachter, L. G. Henry, and R. H. Bragg, J. Appl. Cryst. **21**, 92 (1988).
16. J. B. Aladekomo and R. H. Bragg, Carbon **28**, 897 (1990).
17. M. S. Dresselhaus and G. Dresselhaus, *Light Scattering in Solids III,* edited by M. Cardona and G. Güntherodt (Springer-Verlag, Berlin, Topics in Applied Physics, 1982), Vol. 51, p. 3.
18. F. Tuinstra and J. L. Koenig, J. Chem. Phys. **53**, 1126 (1970).
19. D. S. Knight and W. B. White, J. Mater. Res. **4**, 385 (1989).
20. M. S. Dresselhaus, G. Dresselhaus, K. Sugihara, I. L. Spain, and H. A. Goldberg, *Graphite Fibers and Filaments* (Springer-Verlag, Berlin, Heidelberg, 1988).
21. M. Smíšek and S. Černý, *Active Carbon: Manufacture, Properties and Applications* (Elsevier, New York, 1967); R. E. Franklin, Proc. Roy. Soc. **A209**, 196 (1951).